Molecular Mechanism of the Formic Acid Decomposition on V2O5/TiO2 Catalysts: A Periodic DFT Analysis

ARTICLE *in* THE JOURNAL OF PHYSICAL CHEMISTRY C · OCTOBER 2011

Impact Factor: 4.77 · DOI: 10.1021/jp204652n

2 AUTHORS:

V. I. Avdeev
Boreskov Institute of Catalysis
66 PUBLICATIONS **425** CITATIONS
SEE PROFILE

Valentin N Parmon
Boreskov Institute of Catalysis
526 PUBLICATIONS **5,040** CITATIONS
SEE PROFILE

THE JOURNAL OF PHYSICAL CHEMISTRY C

ARTICLE

pubs.acs.org/JPCC

Molecular Mechanism of the Formic Acid Decomposition on V_2O_5/TiO_2 Catalysts: A Periodic DFT Analysis

Vasilii I. Avdeev* and Valentin N. Parmon

Boreskov Institute of Catalysis, Russian Academy of Science, Novosibirsk 630090, Russian Federation

Supporting Information

ABSTRACT: Molecular and dissociative forms of formic acid adsorption on the V_2O_5/TiO_2 model surface, possible intermediates, and transition states along of the dehydrogenation ($HCOOH \rightarrow CO_2 + H_2$) and dehydration ($HCOOH \rightarrow CO + H_2O$) pathways have been studied by the periodic density functional theory. The CI-NEB analysis of the reaction pathways showed that two types of molecular adsorbed HCOOH species initiate two completely different reaction channels. The first more stable adsorbed form is transformed into the surface formates, which decompose according to the "formate mechanism" to yield products of dehydrogenation, whereas the second weakly adsorbed molecular form decomposes, releasing CO and forming surface hydroxyls. Recombination of two surface hydroxyl groups V−OH to form adsorbed H_2O, followed by water desorption, completes the catalytic dehydration cycle without participation of the formate species. Comparison of the reaction pathways demonstrates that both dehydrogenation and dehydration of formic acid may occur over VO_x/TiO_2 model catalysts with the preferable dehydration pathway.

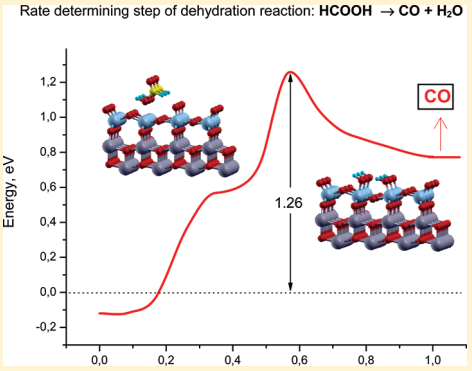

1. INTRODUCTION

Decomposition of formic acid (HCOOH) is the simplest classic reaction in heterogeneous catalysis. This reaction has been thoroughly studied for many years, Mailhe and Sabatier[1] were the first to report the results in their famous paper. The studies of the HCOOH catalytic decomposition were summarized in a number of reviews[2,3] that discussed the decomposition mechanism on metals and bulk metal oxides. It is commonly accepted that the decomposition pathways are controlled by the acid−base properties of the surface sites of oxide catalysts.[4−8] Specifically, dehydrogenation (reaction 1) occurs on typical basic oxides, whereas dehydration (reaction 2) on acidic oxides

$$HCOOH \rightarrow CO_2 + H_2 \quad (1)$$

$$HCOOH \rightarrow CO + H_2O \quad (2)$$

Both reactions proceed at a measurable rate in the easily accessible ranges of temperature and pressure over almost all metal oxides. For this reason, many features of the catalytic decomposition of formic acid are of a special interest for heterogeneous catalysis because decomposition products are possible intermediates of many important oxidation reactions of organic substances. Therefore, the formic acid decomposition can be used as a convenient test reaction to characterize the surface-active sites of metal oxides.[4,9−23]

Among the variety of detected catalytic intermediates, the surface formate ion $HCOO^-$ has been unambiguously identified on various oxides.[14−20,24−26] For this reason, already in the previous works it has been suggested that the decomposition reaction proceeds in general through the dissociative adsorption of formic acid, followed by the formation of a surface formate (SFM) and its decomposition into dehydrogenation or dehydration products

$$HCOOH \rightarrow SFM \rightarrow CO_2 + H_2/CO + H_2O \quad (3)$$

This so-called "formate mechanism" suggests that a high stability of the formate ion governs the overall reaction rate and results in the zero-order kinetics, whereas a low stability of formate corresponds to first-order kinetics. With such kinetic behavior it is possible to explain if a decomposition reaction pathway is present by means of a two-step "volcano curve".[2] However, the "formate mechanism" of decomposition is not universal. As it has been noticed by Trillo et al.[3] a lot of speculations used to approve the participation of surface formats were based on ambiguous correlations. The authors[3] demonstrate some examples where SFM does not participate in the decomposition reaction despite of its existence in the adsorbed phase.

Anyhow, even in those cases where the "formate mechanism" is supposedly valid, one has to take into consideration that the formate decomposition can follow either dehydrogenation or dehydration pathways. Recently, Fein and Wachs[23] examined the dissociative adsorption of formic acid to the surface formate species and their decomposition temperatures (as a measure of the formate thermal stability) over 33 bulk metal oxides including transition-metal oxides V_2O_5, TiO_2, NiO, MoO_3, and WO_3,

Received: May 19, 2011
Revised: September 15, 2011
Published: September 26, 2011

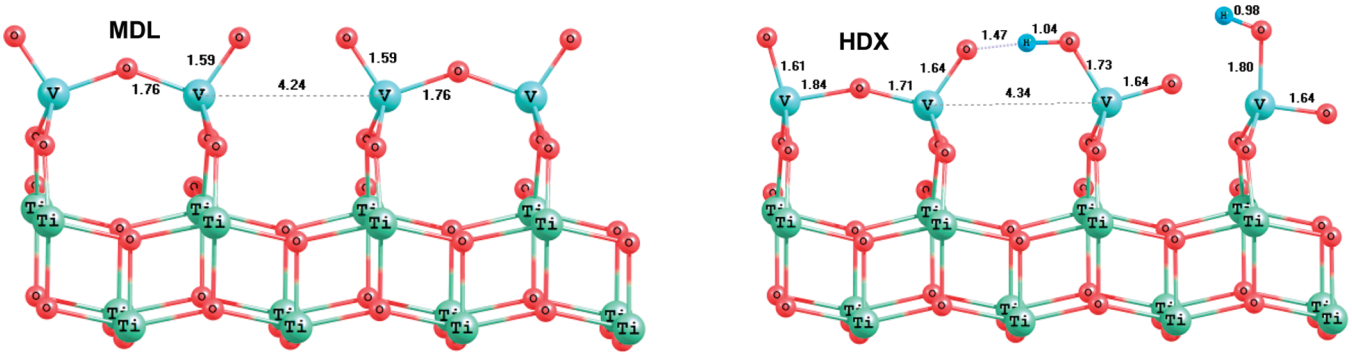

Figure 1. ADM models of the VO_x/TiO_2 catalyst for dehydrated (MDL) and hydroxylated (HDX) surfaces. The coordinates of all atoms in this and the following Figures in XYZ formate are given in the Supporting Information.

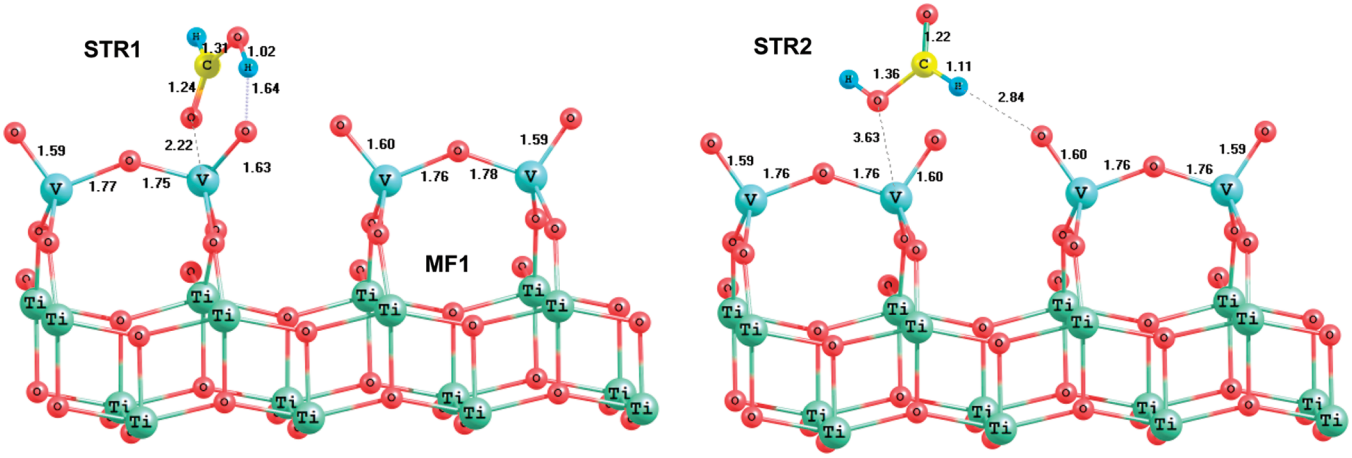

Figure 2. Molecular adsorbed structures of formic acid forming on the fully oxidized VO_x/TiO_2 sites at the HCOOH adsorption via oxygen of C═O carbonyl group (STR1) or oxygen of hydroxyl group (STR2).

which are widely applied in heterogeneous catalysis. Kinetic studies of the formic acid oxidation allowed us to estimate apparent activation energies and suggest some relations between the activity of bulk metal oxide catalysts and their thermodynamic and kinetic parameters. Authors[23] have concluded that the dissociative adsorption of formic acid appears to be not significant for the activity, whereas the thermal stability of the surface formats was found to be an important but not controlling factor for the kinetics. Moreover, the expected classical "volcano shape" dependence of activity versus oxygen bonding strength for the bulk metal oxide catalysts was not observed.

Therefore, the mechanism of the HCOOH decomposition over metal oxide catalysts and, in particular, its elemental steps, the nature of the possible (apart from formate) intermediates, as well as the structure of the decomposition active sites, remain still somewhat mysterious. The detailed molecular mechanism is primarily defined, indeed, by the energy profile along the complete decomposition pathway. The convincing calculations of the reaction ways require reliable models of the oxide catalysts. In this respect, the supported vanadium oxide catalysts are the most reliable model catalysts for fundamental studies of the reaction mechanism.[27] Among a variety of the supported vanadium oxides, the VO_x/TiO_2 catalyst seems to be the most interesting because of its excellent catalytic properties for numerous oxidation reactions.

In the past decade, great progress has been achieved in modeling VO_x/TiO_2 catalytic systems by theoretical DFT methods. Comparison of various low-index surfaces of V_2O_5[28−35] with those of the model catalyst V_2O_5/TiO_2[36−48] demonstrates a dramatic change in the structural and electronic properties of the surface V_2O_5 species due to the existence of strong V−O−Ti interface bonds. Unfortunately, a few of the experimental studies have been devoted only to formic acid decomposition over VO_x/TiO_2 catalysts.[13,49,50] As for theoretical analysis of the formic acid decomposition over metal oxides, the $HCOOH/TiO_2$ seems to be the most thoroughly studied catalyst system.[51−62] However, we failed to find any reports on the formic acid decomposition over V_2O_5/TiO_2 catalysts.

For a deeper understanding of the molecular mechanism of formic acid decomposition, in the present Article, we provide a periodic DFT analysis of electronic structure of possible surface species that are formed via molecular and dissociative adsorption of formic acid on a V_2O_5/TiO_2 catalyst. Two types of molecular adsorbed HCOOH species were found to be formed on the dehydrated V_2O_5/TiO_2 surfaces, which initiate two absolutely different reaction channels. Detailed results of calculations of the reaction pathways are given to identify possible intermediates and transition states that connect these intermediates along the routes of dehydrogenation and dehydration. The dehydrogenation reaction pathway occurs according to the

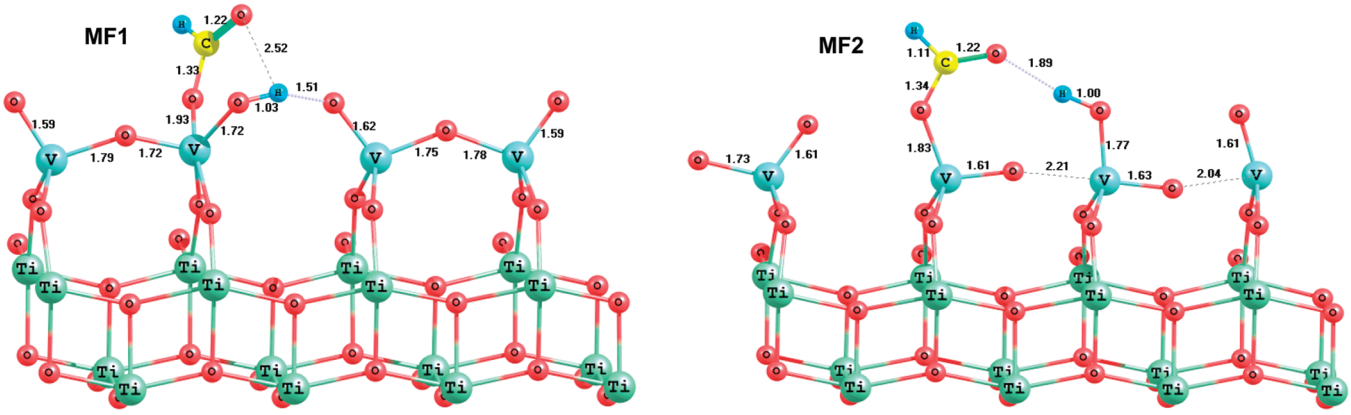

Figure 3. Structures of the surface monodentate formates MF1 and MF2 formed due to dissociative adsorption of formic acid on Lewis acid sites $V^{5+}-O-V^{5+}$.

"formate mechanism" and leads to the SFM interconversion following by desorption of CO_2 and H_2 molecules into the gas phase. By contrast, the dehydration pathway proceeds through the formation of hydroxylated surface with the synchronous elimination of CO molecule to the gas phase without participation of the formate species. The catalytic cycle is completed by the recombination of two hydroxyl groups yielding adsorbed H_2O, followed by its desorption. Both dehydrogenation and dehydration pathways are initiated by the formic acid adsorption on the same Lewis acids sites V^{5+} but proceed via different intermediates. The results obtained provide an important insight into the problem of the molecular mechanism of the formic acid decomposition and the nature of active sites of the titania-supported vanadia catalyst, which are responsible for dehydrogenation and dehydration reactions.

2. COMPUTATIONAL MODELS AND METHODS

The supported vanadium oxide catalyst V_2O_5/TiO_2 was simulated using the (001)-(2 × 4) reconstructed TiO_2 anatase ADM model proposed by Selloni et al.[63,64] Figure 1 shows the models of the dehydrated (MDL) and hydroxylated (HDX) surfaces of V_2O_5/TiO_2 catalyst. The MDL surface is built by the isomorphic replacement of the top surface Ti atoms in the reconstructed layer by V atoms. The resulting supercell (7.56 × 15.12 Å) includes two Ti−O layers and the top V_2O_5 layer with tetrahedrally coordinated V atoms. The hydroxylated surface HDX is formed by dissociative adsorption of water on the dehydrated MDL surface. The resulting surface is appropriate for the 0.5 monolayer OH coverage. The atomic positions of the upper layers were obtained by the structure optimization. For the frozen bottom Ti−O layer, experimental lattice parameters of anatase-TiO_2 were used: $a = b = 3.78$ Å and $c = 9.51$ Å. As seen from Figure 1, the hydroxylation partially blocks the Lewis acids sites and increases the concentration of the Brönsted acid sites V−OH. As a result, the surface V_2O_5 species are exposed to essential reconstruction and the vanadyl oxygen V = O appears to be more reactive in comparison with the dehydrated surface.[43] Details of the construction of resulting models are given elsewhere.[42,43] These MDL and HDX models were accepted as the basis to study structures of the surface intermediates formed on the V_2O_5/TiO_2 catalyst at formic acid decomposition along the dehydrogenation and dehydration pathways.

The calculations were performed with the PWSCF program package[65] based on the spin-polarized density functional theory (DFT). Vanadium, titanium, oxygen, and carbon electron−core interactions were described by the Vanderbilt Ultrasoft pseudopotentials[66] with the exchange-correlation Perdew−Burke−Ernzerhof (PBE) functionals.[67] The wave functions of valence electrons were expanded in plane waves with the kinetic energy cutoff 30 Ry, whereas the charge density cutoff was 120 Ry. The standard energies of the H_2O, CO, CO_2, H_2, and HCOOH molecules were calculated in the Γ point of the Brillouin zone for the tetragonal unit cell with the parameters $a = 10.6$ Å and $c/a = 1.25$. This approach gives the following structure parameters of H_2O molecule: the O−H bond length is 0.98 Å and the H−O−H angle is 104.3°. The calculated C−O bond lengths are 1.14 and 1.18 Å for molecules CO and CO_2, respectively. The reaction pathways were studied by the climbing image nudged elastic band method (CI-NEB).[68−72] Eleven images were specified to locate the start saddle points along the minimum energy path (MEP) with maximal forces<0.06 eV/Å. The final MEP calculations included 17 images for the dehydrogenation and 11 images for the dehydration paths. Figures with the calculated structures presented below were obtained with the ChemCraft[73] and XCrySDen[74] programs.

3. RESULTS AND DISCUSSION

3.1. Molecular and Dissociative Adsorption of Formic Acid on a VO_x/TiO_2 Catalyst. Primarily, we consider the HCOOH adsorption on the MDL surface. Figure 2 shows two possible molecular adsorbed forms of formic acid, STR1 and STR2, on the dehydrated surfaces at HCOOH coverage corresponding to 0.25 monolayer. Configuration STR1 is stabilized by the coordination of the oxygen lone pair electrons of C═O carbonyl group to the Lewis acids site V^{5+}. Configuration STR2 is formed via the coordination of the oxygen of C−OH hydroxyl group to the other V^{5+} sites. The carbonyl oxygen is more basic than the hydroxyl oxygen. Therefore complex STR1 is more stable than STR2. The calculations give for the HCOOH adsorption energy the values of 10.4 and 2.7 kcal/mol for STR1 and STR2, respectively. As it will be shown below, the STR1 decomposition occurs through the surface formates according to dehydrogenation reaction. By contrast, the STR2 decomposition follows in the direction of products of dehydration without the participation of formate species. As follows from Figure 2, the structural

dx.doi.org/10.1021/jp204652n |J. Phys. Chem. C 2011, 115, 21755–21762

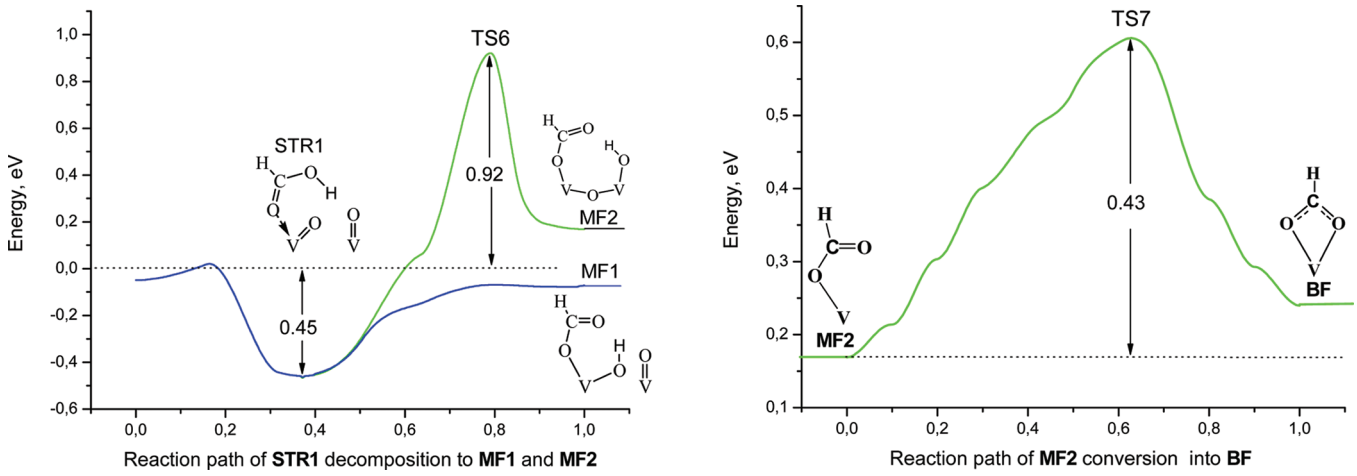

Figure 4. Minimum energy path (MEP) of HCOOH dissociative adsorption on the MDL model surface producing MF1, MF2, and BF formate species. The inset structures of intermediates in this and following Figures show only the neighborhood of one or two vanadia centers. The sum of reactant energies E(HCOOH) + E(MDL) in Figures 4−7 was taken as the reference of a start point of the reaction pathways.

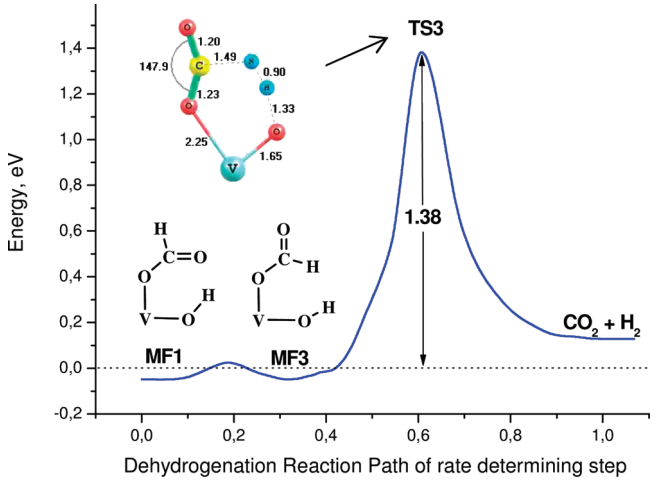

Figure 5. MEP of the MF1 formate decomposition to products of bimolecular dehydrogenation: MF1 →TS3 → CO_2 +H_2. Structure of transition state TS3 is shown in the inset.

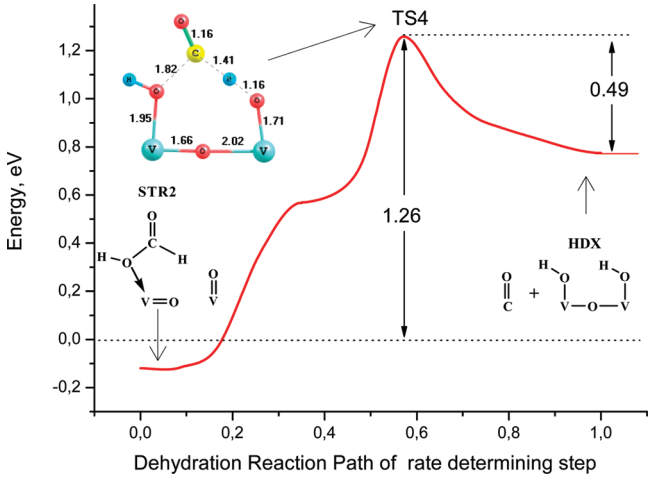

Figure 6. MEP of the HCOOH decomposition leading to CO release into the gas phase and formation of hydroxylated surface HDX. The structure of TS4 transition state is shown in the inset.

configuration of STR1 adsorbed form is associated with the formation of a strong H-bond (the H···O distance is 1.64 Å) between the V = O vanadyl oxygen and proton of HCOOH hydroxyl group. As a result, the hydrogen shift to vanadyl oxygen generates two possible monodentate formate isomers MF1 and MF2 (Figure 3). The structure of MF1 is stabilized via coordination of anions HO^- and $HCOO^-$ on the same V^{5+} Lewis acids site. The structure MF2 is formed if anions HO^- and $HCOO^-$ come into contact with adjacent cations V^{5+}−O−V^{5+}. Monodentate formate MF2 can be converted to bidentate formate structure BF in which two oxygen atoms of formate MF2 are coordinated to the same surface cation V^{5+}. (This configuration is not shown in the Figure.) Formate MF1 is more stable by 4.7 kcal/mol than the MF2 formate being also more stable than BF by 6.3 kcal/mol.

3.2. Reaction Pathway of Bimolecular Dehydrogenation. Figure 4 shows the reaction pathways of the MF1, MF2, and BF formation on MDL surface calculated by CI-NEB method. It can be seen that transformation of formic acid into the surface formate species proceeds via a common intermediate STR1 in two directions. The first path via formate MF2 finishes by the formation of surface bidentate formate BF. This pathway will be analyzed below. The second path through transformation of the surface monodentate formate MF1 leads to products of bimolecular dehydrogenation in two steps (Figure 5). The first step corresponds to the rotation of the functional HCOO group of MF1 around the single C−O bond and leads to stabilization of the mirror isomer MF3 with a negligible energy barrier TS2 = 2.3 kcal/mol. As a result, the V−OCH=O functional group of MF3 orients so that the basic H-atom of the C−H bond directs to the acidic H-atom of V−OH^+ Brönsted acid site, thus causing cleavage of C−H and O−H bonds. The second step corresponds to the activation of V−OCHO bond synchronized with the H atom migration to the H atom of the site V−OH^+ to form bonds O═C═O and H−H. This step proceeds via TS3 transition state and ends by evolution of H_2 and CO_2 molecules into the gas phase. Our calculations give the activation energy of the

dx.doi.org/10.1021/jp204652n |J. Phys. Chem. C 2011, 115, 21755–21762

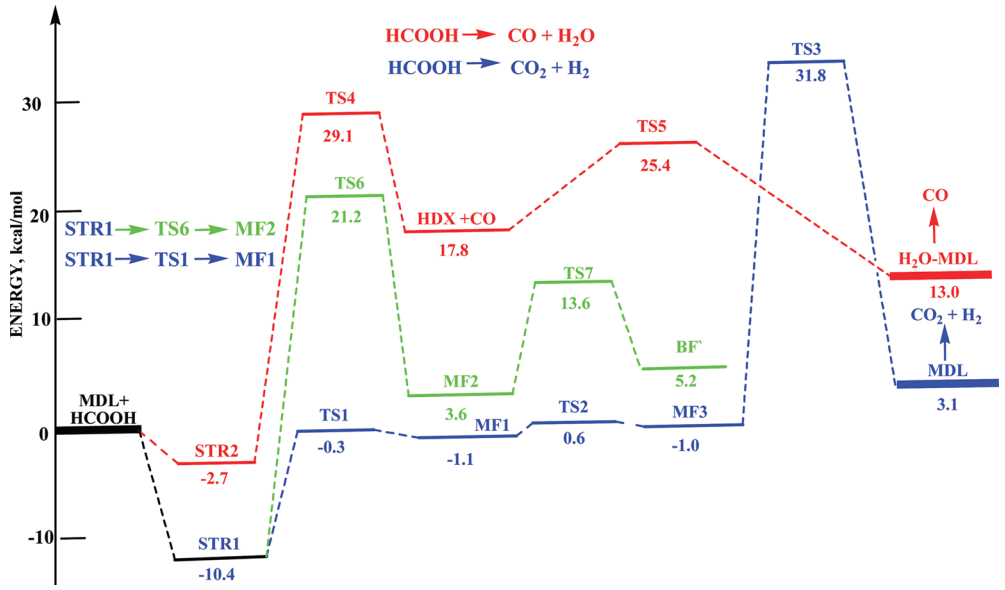

Figure 7. Comparison of the energy pathways of the dehydrogenation HCOOH → $CO_2 + H_2$ and dehydration HCOOH → $CO + H_2O$ reactions on the MDL surface simulating supported V_2O_5/TiO_2 catalyst.

expected rate-determining step the value of 1.38 eV (31.8 kcal/mol), which is comparable to the experimental apparent activation energy, E_{app} = 36 kcal/mol, for the formic acid oxidation over a bulk V_2O_5 catalyst.[23] We may conclude that reaction path, HCOOH + MDL → STR1 → MF1 → MF3 → MDL + CO_2 + H_2, occurs on the Brönsted acid sites V−OH^+ and proceeds via the surface monodentate formate species according to "formate mechanism".

3.3. Reaction Pathway of Monomolecular Dehydration. Now we consider the second HCOOH decomposition pathway. Calculations show that an attack of the tetra-coordinated vanadia site V^{5+} by hydroxyl oxygen of HCOOH along the third-order symmetry axis via the metastable complex STR2 leads to the synchronous cleavage of the C−OH and C−H bonds. These processes via transition state TS4 form the two V−OH hydroxyl groups on the neighboring V^{5+}−O−V^{5+} sites. As a result, CO molecule is evolved into gas phase. This pathway is demonstrated in Figure 6. The initial state is weakly adsorbed HCOOH molecules with STR2 structure shown in Figure 2, whereas the final state corresponds to the hydroxylated surface HDX shown in Figure 1. Subsequent transformation of metastable intermediate HDX has been investigated by us previously in detail.[43] We found that the dehydroxylation pathway via transition state TS5 = 7.6 kcal/mol (accepting energy E(HDX) as the reference) leads to recombination of two surface hydroxyl groups V−OH to form adsorbed H_2O (Figure 7). Therefore, the reaction path, HCOOH + MDL → STR2 → HDX + CO → CO + H_2O-MDL, occurs on the two Lewis acid sites V^{5+}−O−V^{5+} and proceeds through the formation of the hydroxylated surface HDX in direction to the dehydration products without the participation of formate species. The formation of the V−OH hydroxyl groups and generation of mobile protons are thought to be the rate-determining step with activation energy E^* = 1.26 eV (29.1 kcal/mol). Therefore, if the surface contains the hydroxyl groups V−OH initially (for example, through inclusion of water in reaction chamber), it is possible to expect the decrease in activation energy and the increase in the dehydration reaction rate.

At last, the third pathway via the monodentate formate FM2 leads to the formation of bidentate formate STR1 → FM2 → BF in two steps (Figures 4 and 7). The calculations give the activation energy, E^* = 0.92 eV (21.2 kcal/mol), for the first step, and E^* = 0.59 eV (13.6 kcal/mol) for the second one. MF2 and BF surface species coexist with the more stable MF1 formate. Figure 7 demonstrates the energy diagram of the presented above energy pathways in the uniform energy scale. The comparison of the activation energies of two reaction channels STR1 → MF1 → MF3 → TS3 → MDL + CO_2 + H_2 and STR1 → TS6 → MF2 → TS7 → BF shows that the first reaction path seems to be more preferable. We believe that direct participation of a surface formate BF in the HCOOH decomposition processes is hardly probable, but its involvement will not be excluded in the reaction through conversion, BF → MF2 → STR1 → MF1, to the more reactive monodentate formate MF1.

Experimentally, the stable intermediates of molecular and dissociative adsorption of formic acid over the VO_x/TiO_2 catalysts have been identified by in situ IR spectroscopy at temperature ranging from 50 to 200 °C.[49,50] According to this study, the adsorption of formic acid on VO_x/TiO_2 catalysts produces characteristic bands assigned to molecular adsorbed (hydrogen-bonded) HCOOH (1715 cm^{-1}), monodentate formate MF (1668 cm^{-1}), and bidentate formate BF (1370, 1560 cm^{-1}). An experimental kinetic analysis of their subsequent transformation revealed that the temperature elevation up to 100 °C causes disappearance of the hydrogen-bonded complex HCOOH and formation of the MF and BF formate structures. In the temperature range of 100−200 °C, the MF concentration decreases sharply, and BF predominates among the surface species. However, the above spectroscopic data identify only the first and the most stable intermediates, whereas these intermediates cannot be directly related to the further steps of the molecular decomposition reaction paths. In particular, the above data are not decisive for answering the next questions. Do the decomposition reaction paths involve the possible metastable intermediates? Is the decomposition monomolecular or bimolecular? The kinetic model proposed by authors[50] implies decomposition of formic

acid through an only channel HCOOH ↔ BF. They excluded both possible HCOOH → HDX and the most probable HCOOH → MF1 reaction routes. As it can be seen in Figure 7, both the dehydration "no-formate" and the dehydrogenation "formate" pathways of the formic acid decomposition on the VO_x/TiO_2 surface are feasible. Initialization of both dehydrogenation and dehydration pathways occur on the same Lewis acids sites V^{5+} but proceed through different intermediates. The dehydrogenation reaction is regulated by the Brönsted acid site $V-OH^+$. The dehydration reaction goes according to the concert mechanism. The strong basic oxygen sites V = O (rather than the acidic sites V^{5+}) are determinative at the formation of the hydroxylated surface HDX as a rate control step. Very likely, both reactions can compete with each other depending on various reaction conditions. At change of reaction conditions it is possible the switchover the reaction pathways of the dehydrogenation ↔ dehydration.

Recently, Uemura et al.[53,54,58] have demonstrated a similar situation for the catalytic decomposition of HCOOH on the $TiO_2(110)$ surface. On the basis of the DFT calculations with experimental kinetic data, they concluded that at a low temperature and a high HCOOH pressure the dehydrogenation proceeds on Lewis acid sites Ti^{4+}. At high temperature and low HCOOH pressure, the oxygen defect (the oxygen vacancies) is generated on the $TiO_2(110)$ surface, the dehydration reaction path preferably occurs on the basic sites whereas the dehydrogenation path is kinetically suppressed, and there is the switchover of the dehydrogenation → dehydration.

The present results were obtained without consideration of the effect of water on the molecular structure of the surface active sites. Nevertheless, it is possible to define the mode and extent of moisture influence on dehydrogenation and dehydration. As stated above, the appropriate pathways are initiated by the molecular adsorbed forms STR1 and STR2 with adsorption energies 10.4 and 2.7 kcal/mol. The water adsorption energy is 10.2 kcal/mol.[43] Both water and formic acid are adsorbed on identical Lewis acids sites V^{5+}. Water will mainly replace weakly adsorbed STR2 species. As a result, dehydration rate will decreases sharply with increasing water coverage, and the "non-formate mechanism" of CO formation can be completely excluded by the monolayer water coverage. On the contrary, the conjoint adsorption of water and formic acid will lead to an insignificant change in the dehydrogenation reaction rate due to the fact that adsorption energies of formic acid and water are close to one another (10.4 and 10.2, respectively). Therefore, these species will coexist up to the 0.5 monolayer water coverage as one can see in structure STR1. Thus, the selectivity to CO_2, $S_{CO_2} = CO_2/(CO + CO_2)$, will increase, and the selectivity to CO, $S_{CO} = CO/(CO + CO_2)$, will decrease with increasing water coverage.

Finally, the calculated energy profiles of the dehydrogenation and dehydration pathways allow the following feasible scenario of HCOOH decomposition to be suggested. Figure 7 demonstrates that the activation energy of the step STR2 → HDX is so high in comparison with STR2 stability (29.1 and 2.7 kcal/mol) that kinetic aspect will dominate over the thermodynamic one at the HDX formation and its subsequent decomposition steps. On the contrary, STR1 stability (10.4 kcal/mol) is rather high as compared with the activation energies of the steps STR1 → MF1 → MF3 (−0.3 and 2.3 kcal/mol). In this case, it follows to expect that the relative amounts of the surface complexes STR1, MF1, and MF3 are regulated by the thermodynamic factors, but the kinetics (rather than thermodynamics) governs the MF3 decomposition step due to the high activation energy (31.8 kcal/mol). Because the quantum chemical calculations correspond to temperature T = 0 K, from Figure 7 it follows that in a low-temperature limit the complex STR1 should be preferentially transformed into the monodentate formate MF1. At higher temperatures, surface species MF2 and BF seem to coexist with the more stable formate MF1. As the temperature increases, the equilibrium will be shifted toward the endothermic reaction STR1 → MF2 → BF in accordance with the La Chatelier principle. When so, formate species MF1, MF2, and BF may coexist on the catalyst surface, but BF will predominate at the further temperature elevation. This trend agrees with the experimental regularity.[49,50]

In summary, we may say that the successive steps of the HCOOH decomposition proceed according to the "formate mechanism" for the dehydrogenation, and the reaction is governed by the limiting step with activation energy E^* = 31.8 kcal/mol and the enthalpy ΔH = +3.1 kcal/mol. At the same time, the dehydration reaction pathway proceeds without participation of formate species. The limiting step corresponds to the synchronous formation of two Brönsted acid sites $V-OH^+$ with activation energy E^* = 29.1 kcal/mol and the reaction enthalpy ΔH = +17.8 kcal/mol. In accordance with the La Chateiler principle, the low-temperature decomposition of HCOOH gives dehydrogenation products, HCOOH → $CO_2 + H_2$, whereas the temperature elevation results in shifting the equilibrium toward the formation of dehydration products, HCOOH → $CO + H_2O$. These regularities agree well with experimental findings on decomposition of HCOOH over a vanadium−titanium oxide catalyst reported by Elmi et al.[13] They showed that the main reaction product is CO_2 at T < 150 °C but CO at T > 150 °C.

4. CONCLUSIONS

The molecular mechanism of dehydrogenation and dehydration reactions of the formic acid decomposition over model titania-supported vanadia catalyst VO_x/TiO_2 was investigated using the periodic DFT calculations. The corresponding reaction pathways were studied by CI-NEB method. We demonstrated that the dissociative adsorption of HCOOH through the oxygen lone pair electrons of C═O carbonyl group produces surface monodentate formates and V−OH Brönsted acid sites as the initial step of reaction pathway leading to products of bimolecular dehydrogenation, $CO_2 + H_2$. The expected rate-determining step corresponds to migration of the basic H atom of formate to the acidic H atom of $V-OH^+$ Brönsted acid site. The proposed reaction path complies fully to the "formate mechanism". The dehydration pathway is initiated by HCOOH adsorption by the oxygen of C−OH hydroxyl group, followed by the synchronous formation of the hydroxylated surface and evolution of CO molecules into the gas phase. This path is completed by recombination of two V−OH surface hydroxyl groups to form adsorbed H_2O without participation of formate species. The rate-determining step corresponds to the synchronous formation of two $V-OH^+$ Brönsted acid sites. Initialization of both dehydrogenation and dehydration pathways of formic acid decomposition on the VO_x/TiO_2 surface occur on the same Lewis acids sites V^{5+} but proceed through different intermediates. These results are in agreement with experimental findings on the formic acid decomposition over the VO_x/TiO_2 catalyst.[13,49,50]

■ ASSOCIATED CONTENT

Supporting Information. Listing of atomic coordinates for the models and reaction paths discussed. This material is available free of charge via the Internet at http://pubs.acs.org.

■ AUTHOR INFORMATION

Corresponding Author

*E-mail: via@catalysis.nsk.su, via@catalysis.ru. Fax: +7 3832-343056.

■ ACKNOWLEDGMENT

We thank Prof. V. A. Sadykov and Dr. G. A. Popova for many insightful discussions of the obtained results. This work was carried out within the Russian Federal Innovation Agency via the program "Scientific and Educational cadres".

■ REFERENCES

(1) Mailhe, A.; Sabatier, P. *C. R. Acad. Sci.* **1911**, *152*, 1212.
(2) Mars, P.; Scholten, J. J. F.; Zwietering, P. *Adv. Catal.* **1963**, *14*, 35.
(3) Trillo, J. M.; Munuera, G.; Criado, J. M. *Catal. Rev.* **1972**, *7*, 51.
(4) Ai, M. *J. Catal.* **1977**, *50*, 291.
(5) Aramendia, M. A.; Borau, V.; Garcia, I. M.; Jimenez, C.; Marinas, A.; Marinas, J. M.; Porras, A.; Urbano, F. J. *Appl. Catal., A* **1999**, *184*, 115.
(6) Vedrine, J. C. *Top. Catal.* **2002**, *21*, 97.
(7) Patermarakis, G. *Appl. Catal., A* **2003**, *252*, 231.
(8) Ram, B. M.; Ratnam, K. J.; Saikia, P.; Thrimurthulu, G. *J. Mol. Catal. A: Chem.* **2007**, *276*, 197.
(9) Busca, G.; Lorenzelli, V. *J. Catal.* **1980**, *66*, 155.
(10) Peng, X. D.; Barteau, M. A. *Catal. Lett.* **1990**, *7*, 395.
(11) Kim, K. S.; Barteau, M. A. *Langmuir* **1990**, *6*, 1485.
(12) Shido, T.; Asakura, K.; Iwasawa, Y. *J. Catal.* **1990**, *122*, 55.
(13) Elmi, A. S.; Tronconi, E.; Cristiani, C.; Martin, J. P. G.; Forzatti, P.; Busca, G. *Ind. Eng. Chem. Res.* **1989**, *28*, 387.
(14) Petrie, W. T.; Vohs, J. M. *Surf. Sci.* **1991**, *245*, 315.
(15) Onishi, H.; Aruga, T.; Iwasawa, Y. *J. Am. Chem. Soc.* **1993**, *115*, 10460.
(16) Henderson, M. A. *J. Phys. Chem.* **1995**, *99*, 15253.
(17) Henderson, M. A. *J. Phys. Chem. B* **1997**, *101*, 221.
(18) Bandara, A.; Kubota, J.; Wada, A.; Domen, K.; Hirose, C. *Surf. Sci.* **1996**, *364*, L580–L586.
(19) Matsumoto, T.; Bandara, A.; Kubota, J.; Hirose, C.; Domen, K. *J. Phys. Chem. B* **1998**, *102*, 2979.
(20) Bandara, A.; Kubota, J.; Wada, A.; Domen, K.; Hirose, C. *J. Phys. Chem.* **1996**, *100*, 14962.
(21) Xu, C.; Goodman, D. W. *J. Chem. Soc., Faraday Trans.* **1995**, *91*, 3709.
(22) Xu, C.; Goodman, D. W. *Catal. Today* **1996**, *28*, 297.
(23) Fein, D. E.; Wachs, I. E. *J. Catal.* **2002**, *210*, 241.
(24) Altman, E. I.; Tanner, R. E. *Catal. Today* **2003**, *85*, 101.
(25) Dilara, P. A.; Vohs, J. M. *J. Phys. Chem.* **1993**, *97*, 12919.
(26) Yamamoto, H.; Watanabe, N.; Wada, A.; Domen, K.; Hirose, C. *J. Chem. Phys.* **1997**, *106*, 4734.
(27) Muylaert, I.; Van Der Voort, P. *Phys. Chem. Chem. Phys.* **2009**, *11*, 2826.
(28) Chakrabarti, A.; Hermann, K.; Druzinic, R.; Witko, M.; Wagner, F.; Petersen, M. *Phys. Rev. B* **1999**, *59*, 10583.
(29) Yin, X. L.; Han, H. M.; Gunji, I.; Endou, A.; Ammal, S. S. C.; Kubo, M.; Miyamoto, A. *J. Phys. Chem. B* **1999**, *103*, 4701.
(30) Yin, X. L.; Han, H. M.; Endou, A.; Kubo, M.; Teraishi, K.; Chatterjee, A.; Miyamoto, A. *J. Phys. Chem. B* **1999**, *103*, 1263.
(31) Yin, X. L.; Han, H. M.; Miyamoto, A. *Phys. Chem. Chem. Phys.* **2000**, *2*, 4243.
(32) Fu, H.; Liu, Z. P.; Li, Z. H.; Wang, W. N.; Fan, K. N. *J. Am. Chem. Soc.* **2006**, *128*, 11114.
(33) Laubach, S.; Schmidt, P. C.; Thissen, A.; Fernandez-Madrigal, F. J.; Wu, Q. H.; Jaegermann, W.; Klemm, M.; Horn, S. *Phys. Chem. Chem. Phys.* **2007**, *9*, 2564.
(34) Goclon, J.; Grybos, R.; Witko, M.; Hafner, J. *Phys. Rev. B* **2009**, *79*, 075439.
(35) Goclon, J.; Grybos, R.; Witko, M.; Hafner, J. *J. Phys.: Condens. Matter* **2009**, *21*, 095008.
(36) Kachurovskaya, N. A.; Zhidomirov, G. M.; Minot, C. *Surf. Rev. Lett.* **2002**, *9*, 1425.
(37) Calatayud, M.; Mguig, B.; Minot, C. *Surf. Sci.* **2003**, *526*, 297.
(38) Calatayud, M.; Minot, C. *J. Phys. Chem. B* **2004**, *108*, 15679.
(39) Calatayud, M.; Mguig, B.; Minot, C. *Theor. Chem. Acc.* **2005**, *114*, 29.
(40) Calatayud, M.; Minot, C. *Top. Catal.* **2006**, *41*, 17.
(41) Calatayud, M.; Minot, C. *J. Phys. Chem. C* **2007**, *111*, 6411.
(42) Avdeev, V. I.; Tapilin, V. A. *J. Phys. Chem. C* **2009**, *113*, 14941–14945 .
(43) Avdeev, V. I.; Tapilin, V. M. *J. Phys. Chem. C* **2010**, *114*, 3609.
(44) Alexopoulos, K.; Hejduk, P.; Witko, M.; Reyniers, M. F.; Marin, G. B. *J. Phys. Chem. C* **2010**, *114*, 3115.
(45) Grybos, R.; Witko, M. *J. Phys. Chem. C* **2007**, *111*, 4216.
(46) Vittadini, A.; Casarin, M.; Sambi, M.; Selloni, A. *J. Phys. Chem. B* **2005**, *109*, 2176.
(47) Vittadini, A.; Casarin, M.; Selloni, A. *J. Phys. Chem. B* **2005**, *109*, 1652.
(48) Vittadini, A.; Selloni, A. *J. Phys. Chem. B* **2004**, *108*, 7337.
(49) Popova, G. Y.; Chesalov, Y. A.; Andrushkevich, T. V.; Stoyanov, E. S. *React. Kinet. Catal. Lett.* **2002**, *76*, 123.
(50) Ivanov, E. A.; Popova, G. Y.; Chesalov, Y. A.; Andrushkevich, T. V. *J. Mol. Catal. A: Chem.* **2009**, *312*, 92.
(51) Kackell, P.; Terakura, K. *Appl. Surf. Sci.* **2000**, *166*, 370.
(52) Vittadini, A.; Selloni, A.; Rotzinger, F. P.; Gratzel, M. *J. Phys. Chem. B* **2000**, *104*, 1300.
(53) Aizawa, M.; Morikawa, Y.; Namai, Y.; Morikawa, H.; Iwasawa, Y. *J. Phys. Chem. B* **2005**, *109*, 18831.
(54) Morikawa, Y.; Takahashi, I.; Aizawa, M.; Namai, Y.; Sasaki, T.; Iwasawa, Y. *J. Phys. Chem. B* **2004**, *108*, 14446.
(55) Sayago, D. I.; Polcik, M.; Lindsay, R.; Toomes, R. L.; Hoeft, J. T.; Kittel, M.; Woodruff, D. P. *J. Phys. Chem. B* **2004**, *108*, 14316.
(56) Gong, X. Q.; Selloni, A.; Vittadini, A. *J. Phys. Chem. B* **2006**, *110*, 2804.
(57) Vittadini, A.; Casarin, M.; Selloni, A. *Theor. Chem. Acc.* **2007**, *117*, 663.
(58) Uemura, Y.; Taniike, T.; Tada, M.; Morikawa, Y.; Iwasawa, Y. *J. Phys. Chem. C* **2007**, *111*, 16379.
(59) Li, W. K.; Gong, X. Q.; Lu, G.; Selloni, A. *J. Phys. Chem. C* **2008**, *112*, 6594.
(60) Todorova, T.; Peitz, D.; Krocher, O.; Wokaun, A.; Delley, B. *J. Phys. Chem. C* **2011**, *115*, 1195.
(61) Nunzi, F.; De Angelis, F. *J. Phys. Chem. C* **2011**, *115*, 2179.
(62) Miller, K. L.; Musgrave, C. B.; Falconer, J. L.; Medlin, J. W. *J. Phys. Chem. C* **2011**, *115*, 2738.
(63) Lazzeri, M.; Selloni, A. *Phys. Rev. Lett.* **2001**, *87*, 26.
(64) Vittadini, A.; Selloni, A. *J. Phys. Chem. B* **2004**, *108*, 7337.
(65) Giannozzi, P.; Baroni, S.; Bonini, N.; Calandra, M.; Car, R.; Cavazzoni, C.; Ceresoli, D.; Chiarotti, G. L.; Cococcioni, M.; Dabo, I.; Dal Corso, A.; de Gironcoli, S.; Fabris, S.; Fratesi, G.; Gebauer, R.; Gerstmann, U.; Gougoussis, C.; Kokalj, A.; Lazzeri, M.; Martin-Samos, L.; Marzari, N.; Mauri, F.; Mazzarello, R.; Paolini, S.; Pasquarello, A.; Paulatto, L.; Sbraccia, C.; Scandolo, S.; Sclauzero, G.; Seitsonen, A. P.; Smogunov, A.; Umari, P.; Wentzcovitch, R. M. *J. Phys.: Condens. Matter* **2009**, *21*, 395502 .
(66) Vanderbilt, D. *Phys.Rev. B* **1990**, *41*, 7892.
(67) Perdew, J. P.; Burke, K.; Ernzerhof, M. *Phys. Rev. Lett.* **1996**, *77*, 3865.

(68) Henkelman, G.; Uberuaga, B. P.; Jonsson, H. *J. Chem. Phys.* **2000**, *113*, 9901.
(69) Henkelman, G.; Jonsson, H. *J. Chem. Phys.* **2000**, *113*, 9978.
(70) Maragakis, P.; Andreev, S. A.; Brumer, Y.; Reichman, D. R.; Kaxiras, E. *J. Chem. Phys.* **2002**, *117*, 4651.
(71) Mills, G.; Jonsson, H. *Phys. Rev. Lett.* **1994**, *72*, 1124.
(72) Mills, G.; Jonsson, H.; Schenter, G. K. *Surf. Sci.* **1995**, *324*, 305.
(73) ChemCraft, 2010. http://www.chemcraftprog.com/ (accessed Oct 11, 2011).
(74) Kokalj, A. *Comput. Mater. Sci.* **2003**, *28*, 155.